Journal of Power Sources 233 (2013) 269–276

Contents lists available at SciVerse ScienceDirect

Journal of Power Sources

journal homepage: www.elsevier.com/locate/jpowsour

Fabrication and performance evaluation of structurally-controlled PEMFC catalyst layers by blending platinum-supported and stand-alone carbon black

Takahiro Suzuki*, Shohji Tsushima, Shuichiro Hirai

Department of Mechanical and Control Engineering, Tokyo Institute of Technology, 2-12-1-NE-8 Ookayama, Meguro-ku, Tokyo 152-8552, Japan

HIGHLIGHTS

- We fabricated structurally-controlled catalyst layers for PEMFCs.
- Pt loading and thickness of the catalyst layers were successfully controlled.
- Lowering the platinum loading caused a drop in cell performance.
- Thinning the catalyst layer gave better performance.
- Effects of local mass transport in the catalyst layers were investigated.

ARTICLE INFO

Article history:
Received 27 July 2012
Received in revised form
8 November 2012
Accepted 16 January 2013
Available online 26 January 2013

Keywords:
Proton exchange membrane fuel cells
Structurally-controlled catalyst layers
Doctor-blade method
Carbon black
Platinum loading
Local mass transport

ABSTRACT

In proton exchange membrane fuel cells, catalyst layers are key components for achieving higher performance and lower cost. Controlling the structure of the catalyst layers is important, since it can contribute to improving the transport of reactants and products in the catalyst layers, which in turn significantly affects overall potential loss. In this study, we adopted a method of controlling the structure of the catalyst layers by blending platinum-supported and stand-alone carbon black. Catalyst layers in which either thickness or platinum loading were controlled, keeping the other variable constant, were synthesized and evaluated in actual fuel cells. The results showed that lowering the platinum loading caused a drop in cell performance, while thinning the catalyst layer gave better performance. From analyses of the performance evaluations in various conditions, it was indicated that local mass transport (proton and/or oxygen) and water flooding in the catalyst layers plays an important role in cell performance under demanding operating conditions.

1. Introduction

In proton exchange membrane fuel cells (PEMFCs), catalyst layers (CLs) are one of the key components for achieving high performance and overall cost reduction. The synthesis of CLs and catalyst coated membranes (CCMs) has attracted a great deal of research attention to satisfy these demands. However, fundamental understanding is still needed, especially of the synthesizing process, which affects the structure of the CLs and cell performance.

Several typical methods of fabricating CLs are in common use. Categorized by method of application, they are the brush-painting method [1,2], the doctor-blade method [3–5], the screen-printing method [6–8] and the spraying method [9–13]. Processes that are common to these fabrication methods are the blending of materials to produce a slurry called catalyst ink, applying the catalyst ink to form a thin layer, and drying to evaporate the solvents and form a porous medium. There are basically two types of application process. One is by direct-coating onto a polymer electrolyte membrane (PEM) [5,6,8,10–13] and the other is the decal-transfer method, in which the catalyst is applied to a substrate such as a polytetrafluoroethylene (PTFE) sheet. The decal-transfer method requires hot-pressing as an additional fabrication process to form CCMs [1–4,9,14]. These fabrication methods are governed by a number of parameters relating to the materials (e.g., the species and their ratio) and by the details of the fabrication process (e.g., size, time and temperature) that controls the structure of the

* Corresponding author. Tel./fax: +81 3 5734 3554.
E-mail address: suzuki.t.bl@m.titech.ac.jp (T. Suzuki).

0378-7753/$ – see front matter © 2013 Elsevier B.V. All rights reserved.
http://dx.doi.org/10.1016/j.jpowsour.2013.01.092

CLs. To improve the cell performance, these parameters have usually previously been optimized by trial and error. The fabricated CLs, therefore, have a passive structure, which means they have a resultant structure rather than a controlled structure. For active structural control, a fundamental understanding of the processes that create the structure of the CLs and the factors which control this structure is thus required.

The structure and its effects on cell performance have been investigated. Ionomer to carbon weight ratio (I/C), thickness, porosity and Pt loading have been identified as structural parameters. The I/C has a marked effect on the performance of the fuel cell [4,10,15–17]. However, it has been shown that thickness and porosity also change with varying I/C. The thickness and the porosity of the CLs are also important macroscopic structural parameters. Decreasing the thickness can help to reduce overpotential from mass transport, such as of protons and oxygen, since the mass transport distance to the catalyst particles in the CLs is shortened. Porosity also affects the transport of reactant gas and generated water. Reducing Pt loading contributes significantly to reducing the overall cost of the PEMFC systems. However, reducing Pt loading results in degradation of the cell performance. Several attempts have been made to characterize the CLs on a microscopic scale, but development of evaluation methods are still in progress. The structures of ionomers, carbon agglomerates and pores are typical microscopic structural factors. Susac et al. used scanning transmission X-ray microscopy (STXM) to measure ionomer distribution in CLs [18]. Xu et al. investigated the agglomerate structure in catalyst ink using ultra-small-angle X-ray scattering (USAXS) and cryo-transmission electron microscopy (cryo-TEM) [19]. Soboleva et al. evaluated the volumes of primary pores and secondary pores in CLs with various ionomer contents by means of N_2 physisorption measurements [13]. They showed that the volume of primary pores decreased on increasing the Nafion® content, suggesting that the primary pores were coated with ionomer. They also evaluated the cell performance of the CLs [20]. However, the relationship between the microscopic structure and cell performance, which is the macroscopic resultant, remains unclear.

Structural analysis and performance evaluation of the CLs were performed also in our previous study. From the analysis of CLs which have various ionomer to carbon (I/C) weight ratios, it appears that the thickness and porosity of the CLs are chiefly determined by carbon content and ionomer content, respectively [21]. In other words, the thickness and porosity of the CLs made using the conventional CL fabrication process tend to be determined by I/C values. This prompted us to attempt to change these structural parameters positively and focus on the hot-pressing process, which is an important process in the decal-transfer method. The CLs have an elastic deformation range and a plastic deformation range that is a function of the hot-pressing pressure. The pressure, therefore, affects the pore structure of the CLs and the cell performance in the plastic deformation range [22]. However, the thickness of the CLs also varies according to the pressing pressure for the same CL loading. In summary, the structural parameters of the CLs, which are thickness, porosity, I/C, and platinum (Pt) loading, strongly influence each other. It is thus still unclear how each of these structural parameters individually affects cell performance. Methods to control these structural parameters independently, especially the thickness and Pt loading, are needed to evaluate the effects of each parameter on cell performance and to enable future studies on microscopic structures in the CLs to be performed.

Protons, electrons and oxygen are transported to the Pt particles for the oxygen reduction reaction in cathode CLs. The generated water vapor and/or liquid water are then transported outside of the CLs. The recent literature reports that modifying local transport in the CLs has significant potential for improving cell performance [23–26]. Nonoyama et al. reported, based on an analysis of limiting-current measurements, that oxygen permeation through ionomer film is the dominant process of oxygen transport in CLs [25]. Iden et al. measured the proton conductivity of pseudocatalyst layers using the hydrogen pump technique [27,28]. Their results showed proton conductivity to increase with increased RH, in the same way as seen in PEMs, but the values were much lower. Clearly, proton transport in the CLs is an important process, although CLs are much thinner than PEMs. However, the factors in local transport resistance which most significantly affect cell performance under practical operating conditions remain unclear. Under these conditions, water generation can play an important role [29–31]. There is a possibility that water in the CLs affects the local reaction distribution, and the rate-determining process of the reaction can vary according to the operating conditions. Water flooding is an important contributor to performance degradation. However, the location of the sites that most strongly determine the rate-determining process is still not known. Water condensation in the CLs is one of the most likely candidates. The thickness and Pt loading of the CLs are potentially useful parameters for identifying the dominant factor in local transport resistance in the CLs under practical operating conditions.

Platinum-supported carbon (Pt/C) is normally used to fabricate CLs. When using conventional techniques, greater Pt loading causes greater CL thickness [23,32,33]. When using other techniques that vary the Pt to carbon ratio of the Pt/C, there is a concern about the effect of the platinum size [34,35], which complicates experimental analyses of CLs. In this study, we adopted an experimental approach in which we independently controlled the structural parameters of the CLs [26]. We used stand-alone carbon black (CB) and blended it with standard Pt/C to synthesize CLs with specific thicknesses and Pt loading. The objective of this study is to clarify the effects of thickness and Pt loading of the CLs on cell performance under practical operating conditions, focusing specifically on transport phenomena in the CLs.

2. Experimental

2.1. Fabrication and characterization of catalyst layers

TEC10E50E (46.2 wt.% Pt, Tanaka Kikinzoku Kogyo) with a base of Ketjenblack EC was used as Pt/C catalyst and Ketjenblack EC (Lion Corp.) was used as stand-alone CB. The stand-alone CB was preliminary sonicated in ethanol-based solvent to limit agglomerate size. CCMs were fabricated using a typical decal-transfer method. Standard catalyst ink in this study consisted of 20 wt.% Nafion® solution (DE2020, Wako Pure Chemical Industries), Pt/C, water and propanol. The weight percentage of the solid components to the total weight (solid components and volatile components) was 10 wt.%. Stand-alone CB was added as necessary. The ink was mixed in a centrifugal churn for 30 min and then applied to a PTFE sheet using a doctor blade with various blade gaps. After application, the ink was baked at 60 °C for about 10 min. Finally, the ink on the PTFE sheet was transferred to a Nafion® membrane (NRE-212, 50 μm thick, DuPont) by hot-pressing at 140 °C and 0.5 MPa for 10 min. The Pt loading of the CL was measured from the PTFE sheet used to apply the CL. First, the total weight of the PTFE sheet and the catalyst layer was measured using an electric balance. After the hot-pressing, the PTFE sheet was removed from the CL and then the weight of the stand-alone PTFE sheet was measured. The CL loading was calculated from the difference between the two weights. Pt loading was obtained from the weight and mixing ratio of the components. The I/C ratio of the fabricated CLs was fixed at 1.0.

Cross-sectional visualization using scanning electron microscopy (SEM) and N_2 physisorption measurement were performed

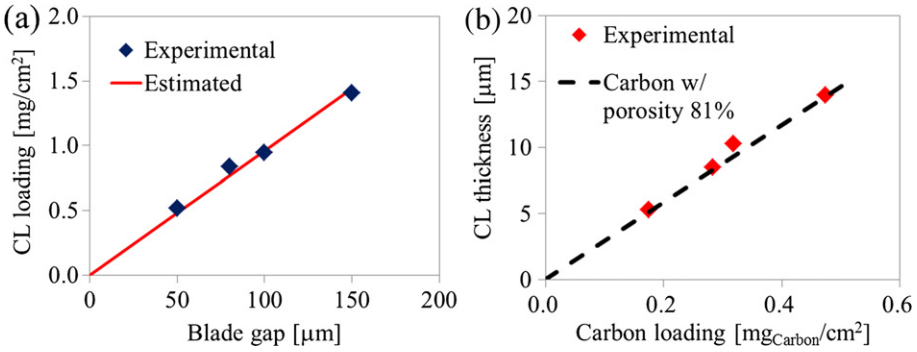

Fig. 1. (a) CL loading at each blade gap and (b) CL thickness at each carbon loading.

to characterize the CLs. Backscattering electron images (BEI) were obtained with an SEM (TM-1000, Hitachi High Tech). The thickness and geometrical porosity of the CLs were obtained by cross-sectional visualization. The geometrical porosity was calculated from the measured thickness and compact thickness, which was obtained from overall weight of the CL, blending ratio and densities of the substances (Densities of carbon, ionomer and platinum are assumed 1.8, 2.0 and 21.45 g cm^{-3}, respectively). N_2 physisorption measurements were performed to obtain pore-size distribution (PSD). Further explanations about the experimental methods have been described in our previous paper [21].

Preliminary investigations to determine the thickness and Pt loading of the CLs with variations in the gap of the doctor blade were performed. We confirmed that CL loading showed a linear increase with blade gap as well as a linear increase of the thickness of the CLs, described as

$$m_{CL} = \alpha t_{gap} \quad (1)$$

$$m_{CL} = \beta t_{gap} \quad (2)$$

where t_{gap} is the blade gap, m_{CL} is CL loading and t_{CL} is the thickness of the CL. α is density of the catalyst ink estimated from the weight ratio of the components and each density. β is a constant that was obtained in preliminary experiments and is a function of the porosity of the CLs.

The thickness and Pt loading in the CLs were independently adjusted by blending Pt/C and stand-alone CB. Pt loading can be described as

$$m_{Pt} = \frac{X_{Pt/CB}}{\left(X_{Pt/CB} + \left(1 + X_{I/CB}\right)\Big/X_{PtC/CB}\right)} m_{CL} \quad (3)$$

where m_{Pt} is Pt loading, $X_{Pt/CB}$ is Pt to CB ratio in the Pt/C, $X_{I/CB}$ is I/C ratio and $X_{PtC/CB}$ is CB in Pt/C to overall CB ratio. Therefore, the t_{gap} and $X_{PtC/CB}$ to obtain targeted Pt loading and the thickness of the CLs are determined by equations (1)–(3).

2.2. Electrochemical measurements

The proton exchange membrane fuel cell we used for operational tests has an active area of 5 cm^2 and a single serpentine channel (1 mm in width, 1 mm in depth). A carbon cloth-type gas diffusion layer (ELAT LT1400W, E-TEK BASF) was used on both sides of the CCMs. The cell operated at 80 °C with H_2 at 200 mL min^{-1} and air or O_2 at 500 mL min^{-1} under ambient pressure during *i–V* measurement. Relative humidity (RH) was set at 40 or 90%. High-frequency resistance at 10 kHz was measured during the *i–V* measurement, employing an AC mΩ tester (Model 356E, Tsuruga Electric Corporation). iR was corrected in the resultant *i–V* curves.

Cyclic voltammetry (CV) was carried out at 30 °C and 100%RH using an electrochemical test system (1280Z-TS, Solartron Analytical). The hydrogen anode was used as a reference electrode. The cathode was filled with N_2 and flow rate was kept to below 50 mL min^{-1} to minimize artifacts [36,37]. The potential was swept from 0.04 to 1.4 V and scan rate was 50 mV s^{-1}.

Total charge for atomic hydrogen adsorption was determined by integrating between a straight baseline drawn from the double layer capacitance region ($E = 0.4$–0.5 V) and the final minimum in the cathodic (negative-going) CV curve. The electrochemically active surface area (ECSA) of the Pt was determined from the hydrogen adsorption charge and the characteristic value of charge density associated with a monolayer of hydrogen adsorbed on polycrystalline platinum, 210 μC cm^{-2}_{Pt}.

3. Results and discussion

3.1. Thickness control using the doctor blade method

To gain a fundamental understanding of thickness determination of the CLs using the doctor-blade method, several CLs were fabricated by varying the blade gap and measured for each CL loading. CL loading can be estimated from the density of catalyst ink, from the densities of each component and the blade gap using equation (1). In this case, α is determined to be 0.096 g cm^{-3}. As shown in Fig. 1(a) as a solid line, the CL loading is expected to vary

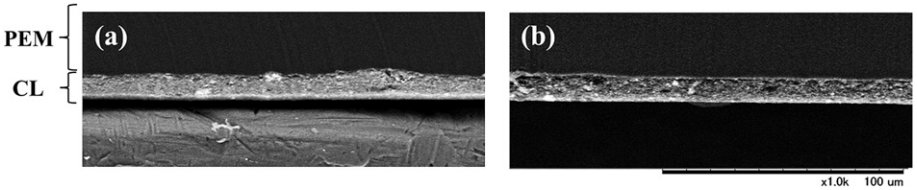

Fig. 2. Cross-sectional SEM images of the CLs. (a) is composed exclusive of CB ($X_{PtC/CB} = 100\%$) and (b) is composed inclusive of CB ($X_{PtC/CB} = 40\%$).

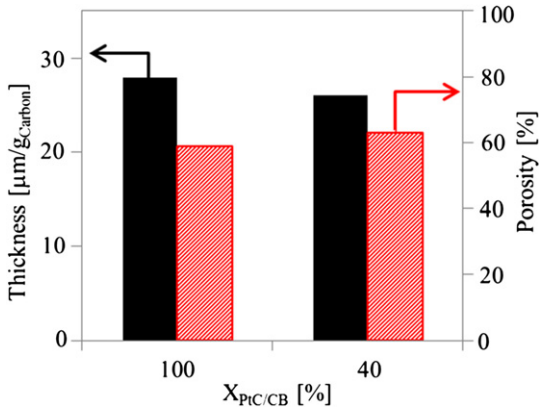

Fig. 3. Thicknesses and porosities of the CLs which are composed exclusive ($X_{PtC/CB}$ = 100%) and inclusive ($X_{PtC/CB}$ = 40%) of CB, respectively.

linearly with change in blade gap. The measurement result, shown as plots in Fig. 1(a) showed linear change as expected. The thickness of the CLs was also measured and showed a linear increase with increased carbon content in the CL (Fig. 1(b)). The thickness of CLs with different I/C values is consistent with this result (data not shown), while a dotted line in the Figure shows the thickness of carbon agglomerates which have a density of 1.8 g cm^{-3} and porosity of 81%. This indicates that CL thickness is chiefly determined by carbon content. This explanation is consistent with our previous study [21]. The results confirm that the CL thickness can be controlled by the doctor blade method.

3.2. Characterization of the CLs inclusive and exclusive stand-alone carbon black

Structural characterization of two CLs, fabricated by applying the same t_{gap} (100 μm), was performed. One was fabricated exclusive of stand-alone CB ($X_{PtC/CB}$ = 100%) and another was fabricated inclusive of it ($X_{PtC/CB}$ = 40%). Fig. 2 shows cross-sectional SEM images of the CLs by BEI. Contrast in BEI depends on atomic number. A bright signal is observed where there are a lot of atoms with high atomic number. The CL exclusive of CB shows a relatively uniform bright image, while the CL inclusive of CB shows uneven brightness. There are two reasons. One is because of the property of the blending CL. The blending CL contains both Pt-supported and stand-alone CB. Therefore, there can be uneven distribution of Pt in several hundreds or tens of nanometer, which means agglomerate size of CB. The other is because of the property of the Pt-supported CB. Pt distribution on the carbon is not even and some carbon agglomerates contains larger Pt than the average. Therefore, there is uneven brightness even in the standard CL. In the CL with the

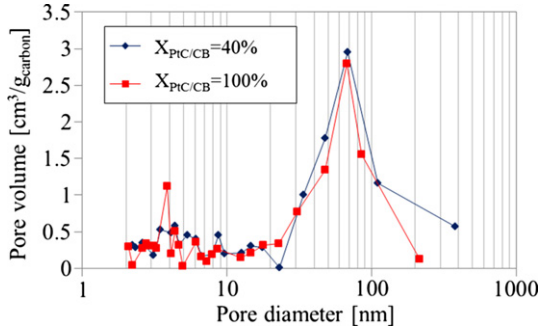

Fig. 4. Pore size distributions of the CLs which are composed exclusive ($X_{PtC/CB}$ = 100%) and inclusive ($X_{PtC/CB}$ = 40%) of CB, respectively.

Table 1
Settings for the thickness-parameter CLs.

t_{gap} [μm]	$X_{PtC/CB}$ [%]	m_{Pt} [mg cm^{-2}]	t_{CL} [μm]
50	100	0.14 ± 0.01	5
100	40		11
150	32		14

Table 2
Settings for the Pt-parameter CLs.

t_{gap} [μm]	$X_{PtC/CB}$ [%]	m_{Pt} [mg cm^{-2}]	t_{CL} [μm]
100	100	0.28	10 ± 1
	40	0.14	
	25	0.07	

stand-alone CB, the uneven brightness becomes more significant because the CL contains agglomerates of stand-alone CB.

Fig. 3 shows thickness per unit carbon content and porosity of the CLs inclusive and exclusive of stand-alone CB obtained from the cross-sectional SEM images. The thickness and porosity of the CL inclusive of CB corresponds to that of the CL exclusive of CB. PSD of the CLs was obtained from nitrogen physisorption measurements, as shown in Fig. 4. PSD of the CL exclusive of CB also corresponds to that of the CL inclusive of CB. These structural analyses confirm that Pt loading of the CLs can be successfully controlled, without varying the other parameters, by blending Pt/C and stand-alone CB.

3.3. Fabrication of structurally-controlled catalyst layers

CLs were fabricated while varying two parameters, t_{gap} and $X_{PtC/CB}$. The results demonstrated that the thickness of the CLs could be varied from 5 to 14 μm without changing the other structural parameters in the CLs (e.g., Pt loading), as shown in Table 1. These CLs are defined as thickness-parameter CLs in this paper. It was also demonstrated that the Pt loading of the CLs could be varied from 0.07 to 0.28 mg_{Pt} cm^{-2} without changing the other structural parameters of the CLs (e.g., thickness), as shown in Table 2. These CLs

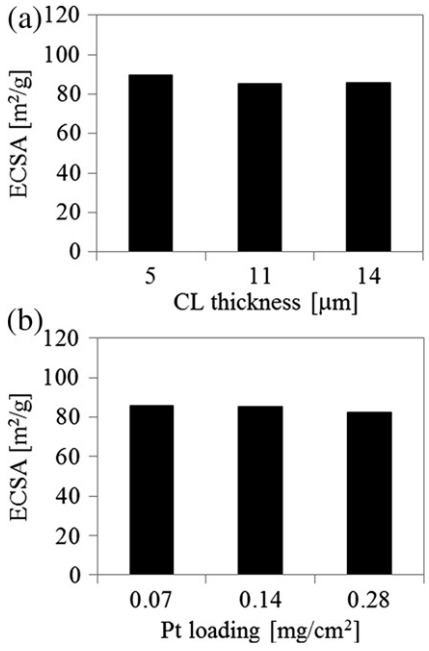

Fig. 5. ECSA of (a) the thickness-parameter CLs and (b) Pt-parameter CLs.

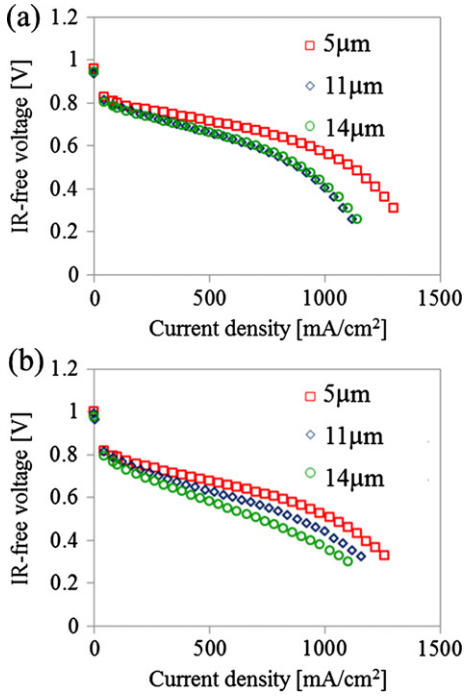

Fig. 6. Cell performances of the thickness-parameter CLs supplying H_2/Air. RH conditions of the cells are (a) 90%RH and (b) 40%RH.

are defined as Pt-parameter CLs in this paper. It is therefore possible to independently investigate the effect of Pt loading and thickness of the CLs on cell performance, as described in the following section.

3.4. Performance evaluation of structurally-controlled catalyst layers

ECSAs of the thickness-parameter CLs and the Pt-parameter CLs are shown in Fig. 5(a) and (b), respectively. These results confirm that CL thickness and Pt loading have no effect on ECSA. In other words, the properties of the catalyst were constant in all CLs in this study, so all the performance differences between them can be attributed to differences in mass transport phenomena.

Polarization curves of the thickness-parameter CLs (Pt loading is fixed at 0.14 mg_{Pt} cm^{-2}) supplied with H_2/Air are shown in Fig. 6. There are two RH conditions: one is 90%RH (Fig. 6(a)) and the other is 40%RH (Fig. 6(b)). The thinnest CL (5 μm) shows better performance than the others due to enhancement of mass transport in the thinner CL. The CLs in low RH conditions (40%RH) show a more marked difference than in high RH conditions (90%RH). In low RH conditions, proton transport in the CLs is poorer than in high RH conditions due to lower proton conductivity [27].

Pt-parameter CLs (CL thickness is fixed at 10 μm) were also evaluated to investigate the effects of local reactant transport. As shown in Fig. 7(a) and (b), the cell performance supplied with H_2/Air deteriorates as Pt loading is reduced in both 90 and 40%RH. Cell performances using the current per Pt weight at each humidity condition are also shown in Fig. 7(c) and (d), respectively. Pt particles in the CL with low Pt loading have to bear larger current than those in the CL with high Pt loading. In other words, each Pt particle has ability to bear such large current even though it results in the large overpotential. Therefore, mass transport can be a rate-determining process. The likely reason is the important role was played by local transport of protons and/or oxygen in the CLs, since the number of Pt particles in the CL decreases as Pt loading is reduced, making each Pt particle bear a higher current, while other structural parameters such as the thickness of the CLs remain constant. To gain a closer understanding of local reactant transport in the CL, we performed two analyses. One was to evaluate ohmic overpotential and the other was to evaluate concentration overpotential.

Fig. 8 shows cell performances of the Pt-parameter CLs supplied with pure oxygen. The measurement range is under 2000 mA cm^{-2}. The polarization curve declines almost linearly from 100 to 2000 mA cm^{-2} and ohmic overpotential is the dominant factor in performance degradation in this range. The degradation becomes more significant at lower Pt loading conditions, as does cell

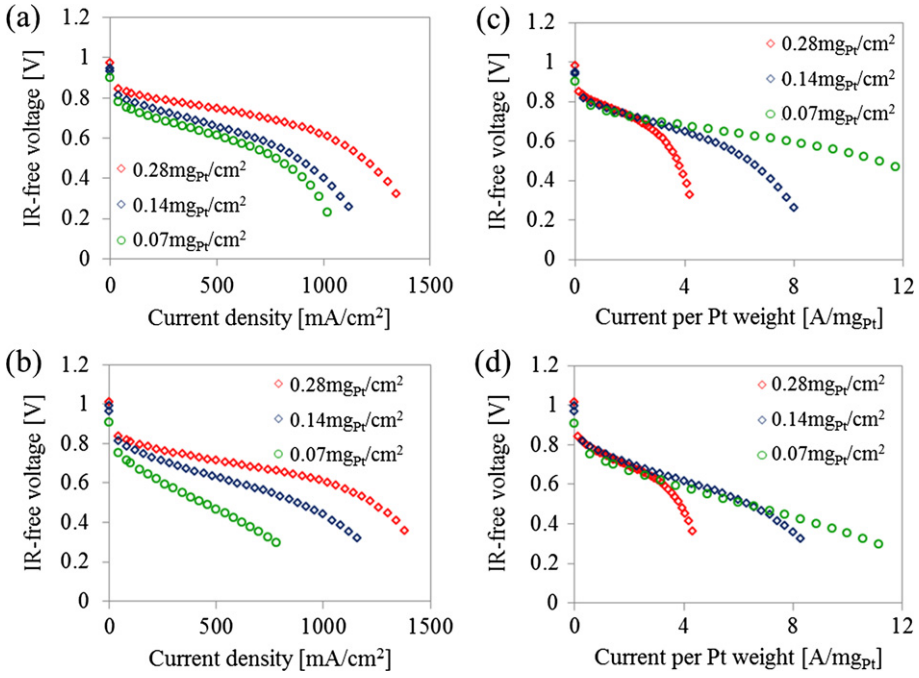

Fig. 7. Cell performances of the Pt-parameter CLs supplying H_2/Air. RH conditions of the cells are (a) 90%RH and (b) 40%RH.

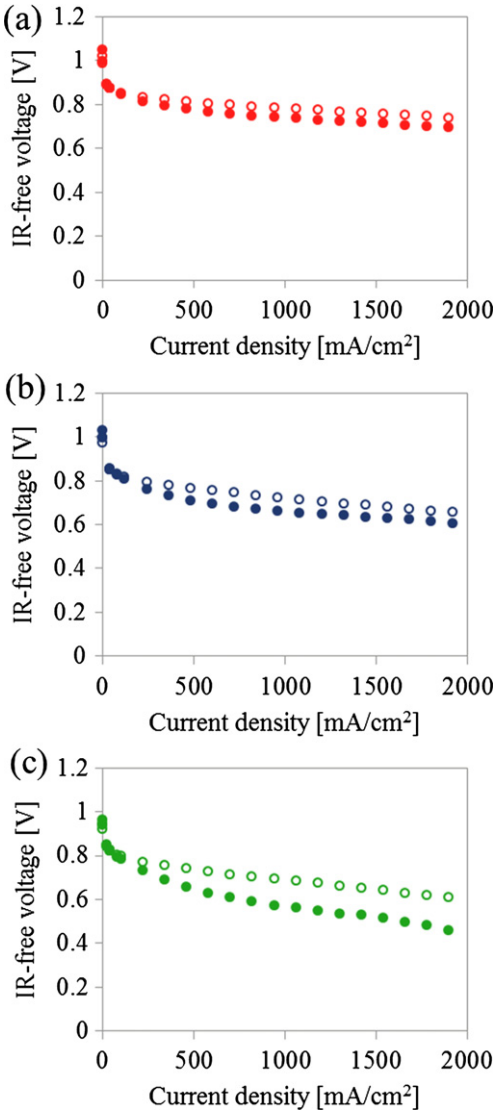

Fig. 8. Cell performances of the Pt-parameter CLs supplying pure oxygen at (a) 0.28 mg_{Pt} cm^{-2}, (b) 0.14 mg_{Pt} cm^{-2} and (c) 0.07 mg_{Pt} cm^{-2}. Open circles and filled circles indicate RH condition of 90%RH and 40%RH, respectively.

performance under air-supplied conditions (Fig. 7). There are two RH conditions: 90%RH and 40%RH in the same Figure for each set of Pt loading conditions. Under all conditions, performance at 40%RH is lower than at 90%RH. The degradation from 90%RH to 40%RH becomes more significant at lower Pt loading, suggesting that ohmic overpotential becomes more significant at lower Pt loading conditions. One of the most likely reasons for ohmic overpotential is proton transport. Proton conductivity decreases as RH in CLs decreases as well as in PEMs [27]. Oxygen permeation through the ionomer is another candidate. However, RH dependency on oxygen permeation in the ionomer is still unclear, although oxygen permeability in the PEM (i.e., the bulk membrane) is positively correlated with RH [38]. Furthermore, if a water film covers the Pt particle surfaces due to water generation, oxygen permeation through water and ionomer films will be poorer under higher RH conditions. This assumption predicts oxygen permeation to be negatively correlated with RH; however, this is contradicted by the performance evaluation results obtained in this study. Further studies on oxygen permeation through the ionomer and/or water film in practical operating conditions are needed.

Polarization deviation was evaluated from the polarization curves to identify concentration overpotential. A linear approximation between 100 and 500 mA cm^{-2} was made and the polarization curve was subtracted from the line. The result was polarization deviation from the linear line, which is a function of concentration overpotential. It was confirmed that the deviation in high RH (90%RH) appears at a lower current density than that in low RH (40%RH), as shown in Fig. 9(a). Under high RH conditions, water flooding appears more readily than in low RH. This evaluation method thus correctly describes the pattern of concentration overpotential which has a relationship with water flooding. A similar evaluation method, known as oxygen gain, has been widely used to evaluate the effect of reactant gas transport on cell performance [39–41]. Oxygen gain is defined as the difference in cell voltage obtained using oxygen and air at a given current density. However, it contains ohmic overpotential, so this method is more suitable for evaluating the effects of CL structure on concentration overpotential than oxygen gain. In the same way, the deviations of the thickness-parameter CLs and the Pt-parameter CLs were evaluated and shown in Fig. 9(a) and (b), respectively. In both cases, the polarization curve supplied with highly humidified (90%RH) H_2/Air was used to evaluate. From these results, it is suggested that Pt loading affects concentration overpotential, whereas CL thickness does not. It has so far been unclear whether CL thickness positively or negatively affects water transport in CLs. A thin CL has the advantage of easy drainage

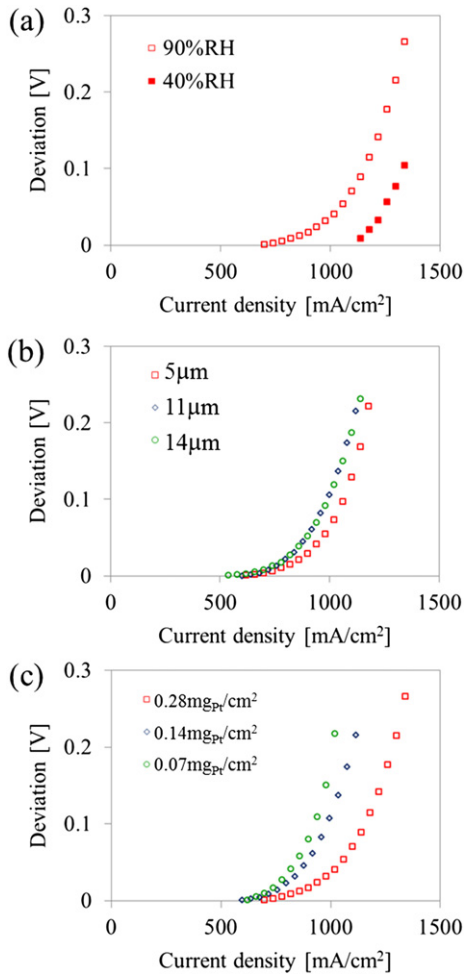

Fig. 9. Polarization deviation of (a) the CL of 10-µm-thickness and 0.28 mg_{Pt} cm^{-2} in 90 and 40%RH, (b) thickness-parameter CLs (H_2/Air, 90%RH) and (c) Pt-parameter CLs (H_2/Air, 90%RH).

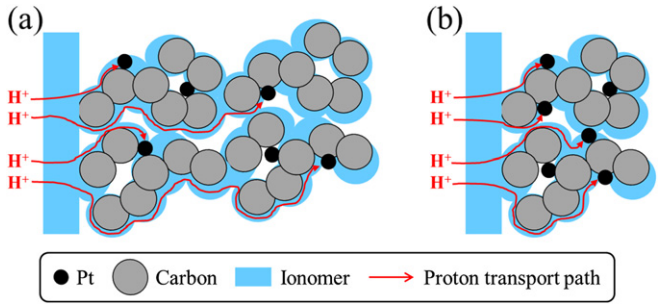

Fig. 10. Schematic of mass transport in (a) thick and (b) thin CLs. Both CLs contain the same number of Pt particles.

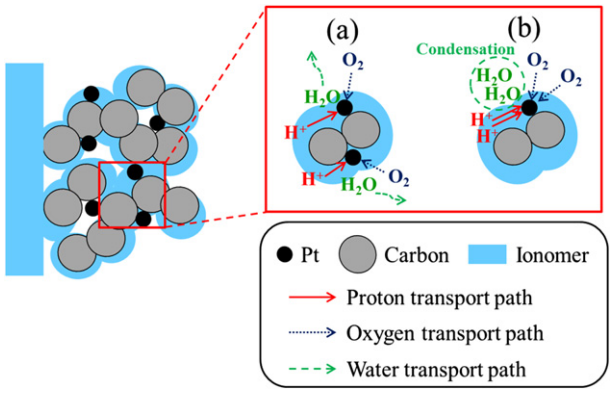

Fig. 11. Schematic of mass transport in (a) high and (b) low Pt-loaded CLs. Both CLs are the same thickness.

outside the CL due to shorter transport distance. On the other hand, it has the disadvantage of being subject to water condensation: a thin CL can contain less generated water than a thick CL, which means that water condenses more easily. This result indicates that these effects are negligible or comparable. A low Pt-loaded CL shows more drastic deviation than with high Pt loading. This is likely to be due to the distinctly local water generation characteristic of CLs.

All the CLs that were fabricated in this study contain the same catalyst (i.e., particle species, size and morphology). The difference between the Pt-parameter CLs is, therefore, only the number of Pt particles, whereas the difference between the thickness-parameter CLs is the average distance of reactant transport to the Pt particles. Fig. 10 shows a schematic of the thickness-parameter CLs. In a thick CL, the average distance of proton and oxygen transport to the Pt particles is longer than in a thin CL. Here, the performance loss has RH sensitivity and the trend corresponds to that of proton conductivity. The longer transport distance results in higher overpotential in the thick CL and demonstrates that proton transport in the CLs is a significant part of the overall process. Fig. 11 shows a schematic of the Pt-parameter CLs. In the low Pt-loaded CL, the number of protons and oxygen transport to each Pt particle are greater for the same current density. This results in higher ohmic overpotential in the low Pt-loaded CL. Furthermore, in the low Pt-loaded CL, water condensation around Pt particles readily occurs, and this phenomenon, which can be called local flooding, can result in higher concentration overpotential.

4. Conclusions

In this study, CL fabrication was performed by blending platinum-supported and stand-alone carbon black to control the thickness and Pt loading and then the CLs in which either thickness or Pt loading were controlled were synthesized and evaluated in a working fuel cell. The effect of local mass transport in the CLs on cell performance in the practical operating conditions was investigated using these structurally-controlled CLs.

Performance evaluation of three types of CLs of different thicknesses (5–14 μm) while keeping the other structural parameters (Pt loading, I/C and porosity) constant was performed. It was clarified that making the CL thinner resulted in better performance. The difference between the CLs is the distance of reactant transport to the Pt particles. A longer transport distance results in a larger ohmic overpotential.

A performance evaluation of three types of CLs with different Pt loading rates (0.07–0.28 mg_{Pt} cm^{-2}) with the other structural parameters (thickness, I/C and porosity) kept constant was also performed. It was clarified that lowering the Pt loading caused deterioration in cell performance. The difference between the CLs is number of Pt particles they contain. In the low Pt-loaded CL, each Pt particle bears a larger current, and this results in a larger ohmic overpotential. Concentration overpotential also increases in the CL because of the local flooding.

These observations clearly indicate that overpotential of the cell is partly attributable to local reactant transport in the CLs. The actual transport distance to the Pt particles and their number are important factors for reducing overall resistance in the cells. In future work, other structural parameters such as I/C and porosity will be fine-tuned to arrive at a closer understanding of local reactant transport phenomena in the CLs. Methods of varying I/C and porosity were established in our previous studies [21,22]. Therefore, this approach will be realized by combining techniques developed in previous studies with those used in this investigation.

Acknowledgments

This work was supported by JSPS KAKENHI Grant-in-Aid for Young Scientists (A) (Grant Number 22686022) and Grant-in-Aid for JSPS Fellows (Grant Number 24009344). The authors are grateful to Lion Corporation for supplying Ketjenblack.

References

[1] J. Xie, K.L. More, T.A. Zawodzinski, W.H. Smith, J. Electrochem. Soc. 151 (2004) A1841.
[2] J. Xie, F. Xu, D.L. Wood Iii, K.L. More, T.A. Zawodzinski, W.H. Smith, Electrochim. Acta 55 (2010) 7404–7412.
[3] G. Bender, T.A. Zawodzinski, A.P. Saab, J. Power Sources 124 (2003) 114–117.
[4] S. Jeon, J. Lee, G.M. Rios, H.-J. Kim, S.-Y. Lee, E. Cho, T.-H. Lim, J. Hyun Jang, Int. J. Hydrogen Energy 35 (2010) 9678–9686.
[5] I.-S. Park, W. Li, A. Manthiram, J. Power Sources 195 (2010) 7078–7082.
[6] J.W. Ihm, H. Ryu, J.S. Bae, W.K. Choo, D.K. Choi, J. Mater. Sci. 39 (2004) 4647–4649.
[7] D.S. Hwang, C.H. Park, S.C. Yi, Y.M. Lee, Int. J. Hydrogen Energy 36 (2011) 9876–9885.
[8] Y.-G. Chun, C.-S. Kim, D.-H. Peck, D.-R. Shin, J. Power Sources 71 (1998) 174–178.
[9] M.S. Wilson, S. Gottesfeld, J. Appl. Electrochem 22 (1992) 1–7.
[10] P. Gode, F. Jaouen, G. Lindbergh, A. Lundblad, G. Sundholm, Electrochim. Acta 48 (2003) 4175–4187.
[11] K.-H. Kim, K.-Y. Lee, H.-J. Kim, E. Cho, S.-Y. Lee, T.-H. Lim, S.P. Yoon, I.C. Hwang, J.H. Jang, Int. J. Hydrogen Energy 35 (2010) 2119–2126.
[12] K.-H. Kim, K.-Y. Lee, S.-Y. Lee, E. Cho, T.-H. Lim, H.-J. Kim, S.P. Yoon, S.H. Kim, T.W. Lim, J.H. Jang, Int. J. Hydrogen Energy 35 (2010) 13104–13110.
[13] T. Soboleva, X. Zhao, K. Malek, Z. Xie, T. Navessin, S. Holdcroft, ACS Appl. Mater. Interfaces 2 (2010) 375–384.
[14] H.-S. Park, Y.-H. Cho, Y.-H. Cho, I.-S. Park, N. Jung, M. Ahn, Y.-E. Sung, J. Electrochem. Soc. 155 (2008) B455.
[15] S. Litster, G. McLean, J. Power Sources 130 (2004) 61–76.
[16] M. Uchida, Y. Aoyama, N. Eda, A. Ohta, J. Electrochem. Soc. 142 (1995) 4143–4149.
[17] E. Antolini, L. Giorgi, A. Pozio, E. Passalacqua, J. Power Sources 77 (1999) 136–142.

[18] D. Susac, V. Berejnov, A.P. Hitchcock, J. Stumper, ECS Trans. 41 (2011) 629–635.
[19] F. Xu, H. Zhang, D. Ho, J. Ilavsky, M. Justics, H. Petrache, L. Stanciu, J. Xie, ECS Trans. 41 (2011) 637–645.
[20] T. Soboleva, K. Malek, Z. Xie, T. Navessin, S. Holdcroft, ACS Appl. Mater. Interfaces 3 (2011) 1827–1837.
[21] T. Suzuki, S. Tsushima, S. Hirai, Int. J. Hydrogen Energy 36 (2011) 12361–12369.
[22] T. Suzuki, S. Tsushima, S. Hirai, ECS Trans. 41 (2011) 909–914.
[23] K. Sakai, K. Sato, T. Mashio, A. Ohma, K. Yamaguchi, K. Shinohara, ECS Trans. 25 (2009) 1193–1201.
[24] K. Kudo, T. Suzuki, Y. Morimoto, ECS Trans. 33 (2010) 1495–1502.
[25] N. Nonoyama, S. Okazaki, A.Z. Weber, Y. Ikogi, T. Yoshida, J. Electrochem. Soc. 158 (2011) B416.
[26] M. Lee, M. Uchida, D.A. Tryk, H. Uchida, M. Watanabe, Electrochim. Acta 56 (2011) 4783–4790.
[27] H. Iden, A. Ohma, K. Shinohara, J. Electrochem. Soc. 156 (2009) B1078.
[28] H. Iden, K. Sato, A. Ohma, K. Shinohara, J. Electrochem. Soc. 158 (2011) B987.
[29] P. Deevanhxay, T. Sasabe, S. Tsushima, S. Hirai, ECS Trans. 41 (2011) 403–408.
[30] P. Deevanhxay, T. Sasabe, S. Tsushima, S. Hirai, ECS 222nd Abstract, 2012, 1487.
[31] P. Deevanhxay, T. Sasabe, S. Tsushima, S. Hirai, Electrochem. Commun. 22 (2012) 33–36.
[32] J. Jiang, B. Yi, J. Electroanal. Chem. 577 (2005) 107–115.
[33] M.S. Saha, D. Malevich, E. Halliop, J.G. Pharoah, B.A. Peppley, K. Karan, J. Electrochem. Soc. 158 (2011) B562.
[34] K. Wikander, H. Ekstrom, A. Palmqvist, G. Lindbergh, Electrochim. Acta 52 (2007) 6848–6855.
[35] W. Sheng, S. Chen, E. Vescovo, Y. Shao-Horn, J. Electrochem. Soc. 159 (2012) B96.
[36] R.N. Carter, S.S. Kocha, F.T. Wagner, M. Fay, H.A. Gasteiger, ECS Trans. 11 (2007) 403–410.
[37] M. Uchimura, S. Kocha, ECS Trans. 11 (2007) 1215–1226.
[38] K. Broka, P. Ekdunge, J. Appl. Electrochem 27 (1997) 117.
[39] Y. Yoon, Int. J. Hydrogen Energy 28 (2003) 657–662.
[40] T.-H. Yang, Y.-G. Yoon, G.-G. Park, W.-Y. Lee, C.-S. Kim, J. Power Sources 127 (2004) 230–233.
[41] M. Prasanna, H.Y. Ha, E.A. Cho, S.A. Hong, I.H. Oh, J. Power Sources 137 (2004) 1–8.